
CBGBench: Fill in the Blank of Protein-Molecule Complex Binding Graph

Haitao Lin^{1,3,†}, Guojiang Zhao^{2,†}, Odin Zhang³, Yufei Huang¹, Lirong Wu¹,
Zicheng Liu¹, Siyuan Li¹, Cheng Tan¹, Zhifeng Gao², Stan Z. Li^{1,*}

¹ AI Lab, Research Center for Industries of the Future, Westlake University;

² Deep Potential; ³ Zhejiang University; [†] Equal Contribution; ^{*} Corresponding Author.

linhaitao@westlake.edu.cn

Abstract

Structure-based drug design (SBDD) aims to generate potential drugs that can bind to a target protein and is greatly expedited by the aid of AI techniques in generative models. However, a lack of systematic understanding persists due to the diverse settings, complex implementation, difficult reproducibility, and task singularity. Firstly, the absence of standardization can lead to unfair comparisons and inconclusive insights. To address this dilemma, we propose CBGBench, a comprehensive benchmark for SBDD, that unifies the task as a generative heterogeneous graph completion, analogous to fill-in-the-blank of the 3D complex binding graph. By categorizing existing methods based on their attributes, CBGBench facilitates a modular and extensible framework that implements various cutting-edge methods. Secondly, a single task on *de novo* molecule generation can hardly reflect their capabilities. To broaden the scope, we have adapted these models to a range of tasks essential in drug design, which are considered sub-tasks within the graph fill-in-the-blank tasks. These tasks include the generative designation of *de novo* molecules, linkers, fragments, scaffolds, and sidechains, all conditioned on the structures of protein pockets. Our evaluations are conducted with fairness, encompassing comprehensive perspectives on interaction, chemical properties, geometry authenticity, and substructure validity. We further provide the pre-trained versions of the state-of-the-art models and deep insights with analysis from empirical studies. The codebase for CBGBench is publicly accessible at <https://github.com/Edapinenut/CBGBench>.

1 Introduction

The rapid and remarkable progress in Graph Neural Networks (GNNs) and generative models have advanced the bio-molecule design in these years [1, 2, 3]. In structure-based drug design, AI-aided methods aim to learn the chemical space of the molecules that can bind to certain proteins as targets, which decreases the general chemical space of molecule compounds ($\sim 10^{60}$) to a more compact search space and enables the model to explore the potential binding drugs. Recent success in generative models such as diffusion models [4, 5, 6] further enhanced these methods to fully exploit the targeted chemical space, and AI-aided SBDD has been propelled into another prominence.

Despite the significance of the SBDD and the development of various approaches, there remains a lack of a comprehensive benchmark for this field covering various practical application scenarios. *On the one hand*, although different methods are proposed for the task, the experimental setup is not unified, and the evaluation protocol also differs. For example, GRAPHBP [7] use a different training and test split of CrossDocked2020 [8] from concurrent works like POCKET2MOL [9] and 3DSBDD [10]; And DIFFBP [11] and GRAPHBP employ Gnina [12] instead of AutoDock Vina [13] as the evaluator for obtaining docking score as binding affinity. Besides, the complex implementation of models makes the

modules coupled, so it is hard to figure out which proposed module contributes to the improvements in performance. For example, though TARGETDIFF [14] and DIFFBP are both diffusion-based methods, the first one uses EGNN [15] to predict the ground-truth position of each atom in the molecule while the later one uses GVP [16] to remove the added noise in a score-based way. To have a systematic understanding of the designation for diffusion models in molecule generation, the network architectures should be fixed to keep the expressivity equal. *On the other hand*, the task of *de novo* generation of molecules is a branch of SBDD. There are also other important tasks, such as the optimization of molecular side chains in lead optimization, or linker design to combine functional fragments into a single, connected molecule [17, 18]. It is highly meaningful to explore whether these methods can be successfully transferred to applications in drug optimization.

In this way, here we propose **CBGBench** as a benchmark for SBDD, with the latest state-of-the-art methods included and integrated into a single codebase (See Appendix. B for details.). Firstly, we unify the generation of the binding molecule as a heterogeneous graph completion task, *i.e.* fill-in-the-blank of the 3D Complex Binding Graph. In this way, the systematic categorization of existing methods is based on three dichotomies: (i) voxelized *v.s.* continuous position generation, (ii) one-shot *v.s.* auto-regressive generation, and (iii) domain-knowledge-based *v.s.* full-data-driven generation. As a result, the methods can be easily modularized and extensible in a unified framework. Secondly, CBGBench introduces a unified protocol with a comprehensive evaluation. In **chemical property**, the classical ones including QED, SA, LogP and LPSK are considered; For **interaction**, besides Vina enery, we extend the evaluation to interaction types between protein and molecules; For **geometry**, we considered static ones including bond length and bond angles, and clashes resulted from protein-molecule cross-clash between atoms in the generated molecules; In **substructure** analysis, we consider single atoms, rings, and functional groups as pharmacophores. Moreover, thanks to our reformulation of the problem and extensible modular implementation, we can easily extend these methods to the other four tasks in lead optimization, including the designation of (i) linkers, (ii) fragments, (iii) side chains and (iv) scaffolds. Comprehensive evaluation is also conducted for these tasks, to explore the potential application value of the existing methods in lead optimization.

As a result, several brief conclusions can be reached as the following:

- CNN-based Methods by using density maps as molecule representations remain highly competitive in target-aware molecular generation.
- For autoregressive methods, it is essential to enable the model to successfully capture the patterns of chemical bonds.
- Prior knowledge has been incorporated into the model in recent works, but the improvements remain limited. Effective design of integrating physical and chemical domain knowledge remains a challenge, leaving substantial room for future research.
- Most evaluated methods can be well generalized to lead optimization. Empirical studies show that scaffold hopping is the most challenging task among them, while linker design is relatively the easiest.
- The conclusions drawn from the experimental results and with the evaluation protocol of CBGBench, are mainly consistent with those obtained on real-world targets, demonstrating generalizability of our benchmark.

2 Background

2.1 Problem Statement

For a binding system composed of a protein-molecule pair as $(\mathcal{P}, \mathcal{M})$, in which \mathcal{P} contains N_{rec} atoms of proteins and \mathcal{M} contains N_{lig} atoms of molecules, we represent the index set of the protein’s atom as \mathcal{I}_{rec} and the molecule’s atoms as \mathcal{I}_{lig} , with $|\mathcal{I}_{\text{rec}}| = N_{\text{rec}}$ and $|\mathcal{I}_{\text{lig}}| = N_{\text{lig}}$. The binding graph can be regarded as a heterogenous graph. One subgraph is protein structures, as $\mathcal{P} = (\mathbf{V}_{\text{rec}}, \mathbf{E}_{\text{rec}})$, where $\mathbf{V}_{\text{rec}} = \{(a_i, \mathbf{x}_i, s_i)\}_{i \in \mathcal{I}_{\text{rec}}}$ is the node set, and $\mathbf{E}_{\text{pa}} = \{(i, j, e_{i,j})\}_{i,j \in \mathcal{I}_{\text{rec}}}$ is the edge set. Here, a_i is the atom types with $a_i = 1, \dots, M$, $\mathbf{x}_i \in \mathbb{R}^3$ is the corresponding 3D position, and $s_i = 1, \dots, 20$ is the amino acid types that i -th atom belongs to; elements in edge set means there exists a bond between i and j , with edge type $e_{i,j}$. The other graph is the molecule structures, written as $\mathcal{M} = (\mathbf{V}_{\text{lig}}, \mathbf{E}_{\text{lig}})$, where $\mathbf{V}_{\text{lig}} = \{(a_i, \mathbf{x}_i)\}_{i \in \mathcal{I}_{\text{lig}}}$ and \mathbf{E}_{lig} is the edge set with the same form as \mathbf{E}_{rec} . Besides, there are virtual edges that exist between protein and molecule,

Table 1: Categorization of included methods. Others except for LiGAN and 3DSBDD model atom positions as continuous variables; Diffusion-based methods maintain a constant atom number in a generation, as one-shot methods; FLAG and D3FG use fragment motifs, and DECOMPDIFF uses arm&scaffolding priors with validity guidance as domain knowledge.

Method	Continuous Position	One-shot Generation	Domain Knowledge
LiGAN	✗	✓	✗
3DSBDD	✗	✗	✗
POCKET2MOL	✓	✗	✗
GRAPHBP	✓	✗	✗
TARGETDIFF	✓	✓	✗
DIFFBP	✓	✓	✗
DIFFSBDD	✓	✓	✗
FLAG	✓	✗	✓
D3FG	✓	✓	✓
DECOMPDIFF	✓	✓	✓

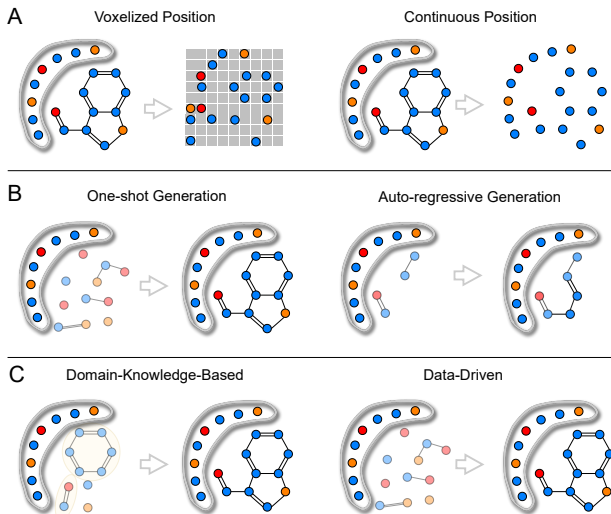


Figure 1: The demonstration of the classification criteria for the existing methods. The gray thick curves outline the contact surface of the protein, and the circles represent different types of atoms.

which make up cross edge set E_{ctx} . Denote the probabilistic model for binding graph by $p(\mathcal{M}, \mathcal{P})$. For the *de novo* molecule generation, the model aims to learn the probability of $p(\mathcal{M}|\mathcal{P})$, as to fill the blank of the protein pocket with a molecule, by using a generative model $p(\cdot)$.

By this means, for the other missing blanks, we write the generation node set as $\mathcal{G} = (\mathbf{V}_{\text{gen}}, \mathbf{E}_{\text{gen}})$, and the molecule context set as $\mathcal{C} = (\mathbf{V}_{\text{ctx}}, \mathbf{E}_{\text{ctx}})$, in which $\mathcal{I}_{\text{ctx}} = \mathcal{I}_{\text{lig}} \setminus \mathcal{I}_{\text{gen}}$. Therefore, the generative model for filling the blank of parts of molecules aims to learn the probability of $p(\mathcal{G}|\mathcal{C}, \mathcal{P})$. The task of fill-in-the-partial-graph is of great significance in SBDD, especially in lead optimization, and we establish other four sub-tasks of it besides *de novo* design, with accessible datasets in Sec. 3.

2.2 Related Work and Taxonomy

The SBDD methods are initially combined with deep neural networks on voxel grids, such as LiGAN [19] generating atom voxelized density maps using VAE [20], and 3DSBDD [10] predicts whether the position on grids is occupied with which type of atoms using auto-regressive models. Then, the development of Equivariant Graph Neural Networks (EGNNs) boosts the SBDD methods to directly generate the continuous 3D positions, such as POCKET2MOL [9] generating the molecules' atom types, positions, and the connected bonds and GRAPHBP [7] employing normalizing flows to generate these attributes, both in an auto-regressive way. The diffusion models [4] further propel the AI-aided SBDD methods, such as TARGETDIFF [14], DIFFBP [11] and DIFFSBDD [21], generating full atoms' positions and element types. Recently, Domain knowledge has been used to constrain or guide the generation of binding drugs. For example, D3FG [22] and FLAG [23] use prior knowledge of fragment motifs to model the coarse structures, and DECOMPDIFF [24] harnesses virtual points searching for arm- and scaffold-clustering as prior knowledge with validity guidance for sampling.

In this way, we can categorize these methods with the three standards:

- Whether the positions of atoms are generated in continuous 3D space or voxelized grids.
- Whether the generation process is auto-regressive or one-shot.
- Whether the domain knowledge is introduced to integrate extra prior into the model.

To better articulate, we classify them according to Table. 1, and Figure. 1 gives a simple demonstration of the criteria for taxonomy.

3 Task and Dataset

Besides the *de novo* molecule generation, the modularized methods can be easily extended to four subtasks which are branches of our defined fill-in-the-blank of the complex binding graph, including

the target-aware linker, fragment, side chain, and scaffold design [25], leading to the generative targets \mathcal{G} for the probabilistic model $p(\mathcal{G}|\mathcal{C}, \mathcal{P})$ to be linkers, fragments, side chains, and scaffolds, and the molecular context \mathcal{C} as the rest. We demonstrate the significance of the four tasks in lead optimization and how the corresponding datasets are established below. The datasets are all established based on previous splits of CrossDocked2020 [8] for fair comparison.

Linker Design. Linker design is a critical strategy in fragment-based drug discovery [26]. It focuses on creating linkers that connect two lead fragments and obtaining a complete molecule with enhanced affinity. Effective linker design can significantly influence the efficacy and pharmacokinetics of the drug, by ensuring that the molecule maintains the desired orientation and conformation when bound to its target [27]. We define linkers following specific rules: (i) A linker should act as the intermediate structure connecting two fragments. (ii) A linker should contain at least two atoms on the shortest path between two fragments. (iii) Each connecting fragment must consist of more than five atoms.

Fragment Growing. Fragment growing also plays an important role in fragment-based drug design, focusing on expanding a fragment on the lead compound to better fill the binding pocket [28]. It also relates to adjusting pharmacological properties, such as enhancing solubility or reducing toxicity [29]. In this approach, we decompose the entire ligand into two fragments and select the smaller one for expansion based on specific criteria: (i) Each fragment must contain more than five atoms. (ii) The smaller fragment should be larger than half the size of the larger one.

Side Chain Decoration. Side chain decoration overlaps with fragment growing but differs in that it permits modifications at multiple sites on the lead compound, whereas fragment growing typically modifies a single site. The taxonomy of arms-scaffold in some previous work [30] is similar to side-chain-scaffold, while we focus on a chemist-intuitive approach, Bemis-Murko decomposition [31], which treats all terminal non-cyclic structures as side chains.

Scaffold Hopping. Scaffold hopping is introduced by Schneider [32], as a strategy in medicinal chemistry aiming to replace the core structure of molecules to explore more diverse chemical structures or improve specific properties. While various empirical definitions exist [33], for consistency, the Bemis-Murko decomposition is utilized to define the scaffold structure.

Since chances are that there is no substructure in a molecule according to the discussed definition of the decomposition, we here give the instance number of training and test set for each task in Table. 2.

4 Evaluation Protocol

In previous works, the evaluation usually focuses on two aspects including **interaction** and **chemical property**. We extend them and add another two standards on molecule 3D structure’s authenticity with **geometry** analysis and the 2D graphs reliability with **substructure** analysis, as the following:

Substructure. To evaluate whether the model succeeds in learning the 2D graph structures for drug molecules. We expand previous metrics to functional groups, as certain functional groups in the drugs act as pharmacophores, such as phenol and pyrimidine. We identify the 25 most frequently occurring functional groups by using EFG [34] (Appendix. A.1 gives the details), and calculated mean frequency of each function group generated in a molecule and the overall multinomial distribution. In the same way, the two values can also be obtained according to rings and atom types. The generated frequency and distribution against the references lead to 6 metrics on substructure analysis including (i) $\text{JSD}_{\text{at}}(\downarrow)$, (ii) $\text{MAE}_{\text{at}}(\downarrow)$, (iii) $\text{JSD}_{\text{rt}}(\downarrow)$, (iv) $\text{MAE}_{\text{rt}}(\downarrow)$, (v) $\text{JSD}_{\text{fg}}(\downarrow)$, and (vi) $\text{MEA}_{\text{fg}}(\downarrow)$, where ‘at’ means atom type, ‘rt’ means ring type and ‘fg’ means functional group.

Chemical Property. We continue the evaluation of chemical properties from most previous works, including (i) $\text{QED}(\uparrow)$ as quantitative estimation of drug-likeness; (ii) $\text{SA}(\uparrow)$ as synthetic accessibility score; (iii) LogP represents the octanol-water partition coefficient, and in general LogP values should be between -0.4 and 5.6 to be good drug candidates [35]; (iv) $\text{LPSK}(\uparrow)$ as the ratio of the generated drug molecules satisfying the Lipinski’s rule of five.

Interaction. In evaluating the generated molecules’ interaction with proteins, the binding affinity is usually the most important metric. Here we unify the affinity calculation with AutoDock Vina for fair comparison. However, previous studies show that larger molecule sizes will lead to a higher probability that the generated molecules can make interaction with the protein, resulting in higher predicted binding affinity [36, 37]. It is also an observation in this paper as the Pearson correlation of Vina Energy v.s. atom number reaches -0.67 (See Appendix. A.2). Besides, in some structures, there

Table 2: The instance number of training and test split in the datasets for the four tasks and *De novo* generation. The decomposition is conducted in the training and test set of CrossDocked2020 to avoid label leakage. Side chain decoration and scaffold hopping are two dual tasks, so the training and test set numbers are the same.

Dataset	# Training	# Test
<i>De novo</i>	99900	100
Linker	52685	43
Fragment	61379	61
Side Chain	70617	64
Scaffold	70617	64

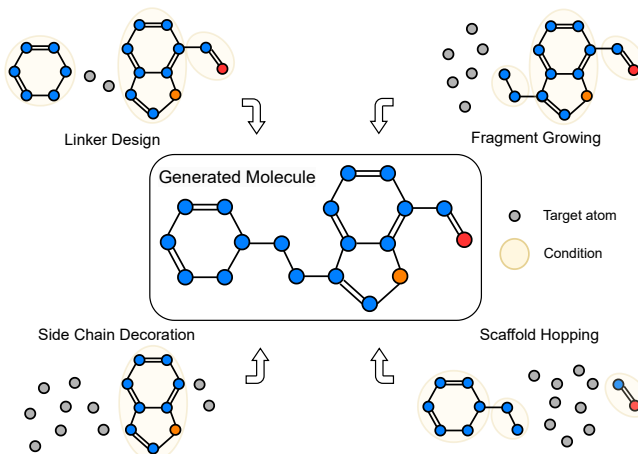


Figure 2: Demonstration of the four tasks.

are more atoms in the protein participating in the interaction, which also causes the average to be unreasonable. Therefore, besides the commonly-used (i) E_{vina} (\downarrow) as the mean Vina Energy, and (ii) $IMP\%$ (\uparrow) as the improvements indicating the ratio of the generated molecule with lower binding energy than the reference, we use mean percent binding gap as (iii) $MPBG$ (\uparrow) (Appendix. A.3 gives computation) and ligand binding efficacy as (iv) LBE (\uparrow), written as $LBE_i = -\frac{E_{vina}}{N_{lig}}$, indicating how much does a single atom in the molecule contribute to the binding affinity, to eliminate the effects of molecule sizes. Moreover, it is important for the generated molecules to keep the same or similar interaction patterns with proteins [38]. Therefore, we aim to figure out whether the SBDD models can learn the microscopic interaction patterns hidden in the data of the 3D conformations. We use PLIP [39, 40, 41] to characterize the 7 types of interactions, and calculate per-pocket and overall Jensen-Shannon divergence (JSD) between the categorical distributions of generated types and reference types and mean absolute error (MAE) between the frequency of each generated types v.s. it of reference types, in which the frequency is defined as the average number of occurrences of each type of interaction produced by different single generated molecules binding to the same protein, leading to four metrics including (v) JSD_{PP} (\downarrow), (vi) JSD_{OA} (\downarrow), (vii) MAE_{PP} (\downarrow), (viii) MAE_{OA} (\downarrow), where ‘PP’ and ‘OA’ means per-pocket and overall respectively.

Geometry. The internal geometry is an important characteristic for distinguishing between general point clouds and molecular structures. The torsion angles [42, 43] are flexible geometries, while bond lengths and bond angles are static to reveal whether the generated molecules have realistic structures. Hence, we evaluate the overall JSD of bond length and angle distribution between reference and generated ones, written as (i) JSD_{BL} (\downarrow) and (ii) JSD_{BA} (\downarrow). The other perspective for validating structural resonability is the clash, the occurrence of which is defined when the van der Waals radii overlap by $\geq 0.4\text{\AA}$ [44]. Hence, the ratio of number of atoms generating clashes with protein atoms to the total atom number is written as (ii) $Ratio_{cca}$ (\downarrow) (cross clashes at atom level). Besides, the ratio of molecules with clashes as $Ratio_{cm}$ (\downarrow) (molecule with clashes) are evaluated.

The four designation tasks are shown in Figure. 2. We here evaluate the 10 methods in Table. 1, and use Friedman rank [45, 46, 47] as the mean ranking method, to fairly compare the performance of different models in the four aspects. The ranking score is calculated by $(10 - \text{rank})$, and the final rank is according to the weighted mean ranking score. Appendix. A.3 gives computation of the metrics.

5 Benchmark Result

5.1 *De novo* Generation

5.1.1 Setup

Training. We use the default configuration in each model’s released code base as the hyperparameter, and set the training iteration number as 5,000,000 for fair comparison. It is noted that the loss of autoregressive methods exhibits a faster convergence rate of loss, typically requiring only a few tens of thousands of epochs to reach the final best checkpoint. To eliminate the effect brought about

Table 3: Results of substructure analysis.

Methods	Metrics		Atom type		Ring type		Functional Group		Rank
	JSD _{at}	MAE _{at}	JSD _{rt}	MAE _{rt}	JSD _{fg}	MAE _{fg}			
LIGAN	0.1167	0.8680	0.3163	0.2701	<u>0.2468</u>	<u>0.0378</u>	4.67		
3DSBDD	0.0860	0.8444	0.3188	0.2457	0.2682	0.0494	4.67		
GRAPHBP	0.1642	1.2266	0.5061	0.4382	0.6259	0.0705	9.33		
POCKET2MOL	0.0916	1.0497	0.3550	0.3545	0.2961	0.0622	6.67		
TARGETDIFF	<u>0.0533</u>	0.2399	<u>0.2345</u>	0.1559	0.2876	<u>0.0441</u>	2.50		
DIFFSBDD	<u>0.0529</u>	<u>0.6316</u>	0.3853	0.3437	0.5520	0.0710	6.50		
DIFFBP	0.2591	1.5491	0.4531	0.4068	0.5346	0.0670	8.83		
FLAG	0.1032	1.7665	0.2432	0.3370	0.3634	0.0666	6.83		
D3FG	0.0644	0.8154	0.1869	<u>0.2204</u>	<u>0.2511</u>	0.0516	<u>3.33</u>		
DECOMPDIFF	0.0431	<u>0.3197</u>	<u>0.2431</u>	<u>0.2006</u>	0.1916	0.0318	1.67		

Table 4: Results of chemical property.

	QED	LogP	SA	LPSK	Rank
LIGAN	0.46	0.56	0.66	4.39	4.00
3DSBDD	<u>0.48</u>	0.47	0.63	4.72	<u>3.00</u>
GRAPHBP	0.44	3.29	<u>0.64</u>	4.73	3.25
POCKET2MOL	0.39	2.39	<u>0.65</u>	4.58	4.00
TARGETDIFF	0.49	1.13	0.60	4.57	3.50
DIFFSBDD	0.49	-0.15	0.34	<u>4.89</u>	<u>3.00</u>
DIFFBP	<u>0.47</u>	5.27	0.59	4.47	4.50
FLAG	0.41	0.29	0.58	4.93	3.75
D3FG	0.49	1.56	0.66	<u>4.84</u>	1.50
DECOMPDIFF	0.49	1.22	0.66	4.40	<u>3.00</u>

Table 5: Results of interacton analysis.

Methods	Metrics		Vina Score		Vina Min		Vina Dock				PLIP Interaction				Rank
	E_{vina}	IMP%	E_{vina}	IMP%	E_{vina}	IMP%	MPBG%	LBE	JSD _{OA}	MAE _{OA}	JSD _{PP}	MAE _{PP}			
LIGAN	-6.47	62.13	-7.14	70.18	-7.70	72.71	4.22	<u>0.3897</u>	0.0346	0.0905	<u>0.1451</u>	0.3416	2.33		
3DSBDD	-	3.99	-3.75	17.98	-6.45	31.46	9.18	0.3839	0.0392	0.0934	0.1733	0.4231	5.75		
GRAPHBP	-	0.00	-	1.67	-4.57	10.86	-30.03	0.3200	0.0462	0.1625	0.2101	0.4835	9.33		
POCKET2MOL	<u>-5.23</u>	<u>31.06</u>	-6.03	<u>38.04</u>	-7.05	48.07	-0.17	0.4115	0.0319	0.2455	<u>0.1535</u>	<u>0.4152</u>	<u>4.16</u>		
TARGETDIFF	<u>-5.71</u>	<u>38.21</u>	<u>-6.43</u>	<u>47.09</u>	<u>-7.41</u>	<u>51.99</u>	<u>5.38</u>	0.3537	<u>0.0198</u>	<u>0.0600</u>	0.1757	0.4687	<u>3.08</u>		
DIFFSBDD	-	12.67	-2.15	22.24	-5.53	29.76	-23.51	0.2920	0.0333	0.1461	0.1777	0.5265	7.42		
DIFFBP	-	8.60	-	19.68	<u>-7.34</u>	<u>49.24</u>	<u>6.23</u>	0.3481	0.0249	0.1430	0.1256	0.5639	5.67		
FLAG	-	0.04	-	3.44	-3.65	11.78	-47.64	0.3319	0.0170	<u>0.0277</u>	0.2762	<u>0.3976</u>	7.50		
D3FG	-	3.70	-2.59	11.13	-6.78	28.90	-8.85	<u>0.4009</u>	0.0638	0.0135	0.1850	0.4641	6.67		
DECOMPDIFF	-5.18	19.66	<u>-6.04</u>	34.84	-7.10	48.31	-1.59	0.3460	<u>0.0215</u>	0.0769	0.1848	0.4369	4.58		

by the architecture of GNNs, in implementation, we use GVP [16] and EGNN [15] with GAT [48], as message-passing modules of auto-regressive and diffusion-based models, respectively. Especially, the GNN for encoding and decoding functional groups in D3FG is a combination of GAT and LoCS [49], and CNN for processing atom density maps is four convolution blocks in LIGAN.

Evaluation. Following the previous protocol, we generate 100 molecules per pocket in the test set, while not all the generated molecules are chemically valid (See Appendix. C.3), which will lead to <10,000 molecules. In affinity evaluation, we employ three modes of AutoDock Vina, including ‘Score’, ‘Minimize’, and ‘Dock’. MPBG and LBE are added to the Vina Dock mode. For Vina energy that is larger than 0, we think it is invalid, so we will not report it, and give the lowest ranking in the column of metrics. Moreover, LogP only provides a reference range for drug molecules, so we assigned a rank of 1 to the generated molecules within the range and 2 to those outside the range. In all the tables, values in **bold** are the best metric, and values with underline are the second and third.

5.1.2 Result Analysis

Substructure. Table. 3 gives results on 2D substructures (For details, see Appendix. C.1.1).

(i) Overall, the auto-regressive models perform worse than the one-shot ones, especially in ring-type evaluation, where the former ones are more likely to generate triangular and tetrahedral rings. (ii) TARGETDIFF, DIFFSBDD and DECOMPDIFF exhibit advantages in atom type. DIFFBP has difficulties in generating atoms with low occurrence frequencies. (iii) DECOMPDIFF and D3FG exhibit advantages due to the incorporation of prior knowledge in ring types and functional groups. DIFFBP and DIFFSBDD perform poorly due to inconsistencies in generating complex fragments.

Chemical Property. The chemical property is calculated with 2D molecule graphs, so it can be greatly influenced by the molecule substructures. From Table. 4, we can conclude that (i) In terms of the four metrics, the differences among the compared methods are not significant. (ii) D3FG shows the best overall properties, with the highest QED, SA, and LPSK.

Interaction. From Table. 5 shows that (i) LIGAN as a CNN-based method generates molecules that are initialized with high stability according to its superior performance in Vina Score and Vina Min. It also performs well in Vina Dock mode, with a positive MPBG and high LBE, providing good consistency in interaction patterns. (ii) Auto-regressive methods except POCKET2MOL can hardly capture the pocket conditions and generate stably-binding molecules well, with very low IMP% in all Vina modes, while POCKET2MOL is the state-of-the-art auto-regressive method in *de novo* generation. (iii) In diffusion-based methods, TARGETDIFF outperforms the other competitors in overall interaction comparison, and DECOMPDIFF performs competitively since the difference between these two methods is actually minimal. DIFFBP’s performance in docking mode is comparable, but in other modes, it performs less satisfactorily. Performance of DIFFSBDD is less than satisfactory. D3FG

Table 6: Results of geometry analysis.

Methods	Metrics		Static Geometry		Clash		Rank
	JSD _{BL}	JSD _{BA}	Ratio _{cca}	Ratio _{cm}			
LIGAN	0.4645	0.5673	0.0096	0.0718	4.75		
3DSBDD	0.5024	0.3904	0.2482	0.8683	6.75		
GRAPHBP	0.5182	0.5645	0.8634	0.9974	9.50		
POCKET2MOL	0.5433	0.4922	0.0576	0.4499	6.50		
TARGETDIFF	<u>0.2659</u>	<u>0.3769</u>	0.0483	0.4920	<u>3.00</u>		
DIFFSBDD	0.3501	0.4588	0.1083	0.6578	5.25		
DIFFBP	<u>0.3453</u>	0.4621	<u>0.0449</u>	<u>0.4077</u>	<u>3.25</u>		
FLAG	0.4215	0.4304	0.6777	0.9769	7.00		
D3FG	0.3727	0.4700	0.2115	0.8571	6.50		
DECOMPDIFF	0.2576	0.3473	<u>0.0462</u>	0.5248	2.50		

Table 7: Ranking scores and overall ranking.

Methods	Weights	Substruc.	Chem.	Interact.	Geom.	Rank
	0.2	0.2	0.4	0.2		
LIGAN	1.07	1.20	3.07	1.05	<u>3</u>	
3DSBDD	1.07	1.40	1.70	0.65	6	
GRAPHBP	0.13	1.35	0.27	0.10	10	
POCKET2MOL	0.67	1.20	2.34	0.70	5	
TARGETDIFF	1.50	1.30	2.77	1.40	1	
DIFFSBDD	0.70	1.40	1.03	0.95	8	
DIFFBP	0.23	1.10	1.73	1.35	7	
FLAG	0.63	1.25	1.00	0.60	9	
D3FG	1.33	1.70	1.33	0.70	4	
DECOMPDIFF	1.67	1.40	2.17	1.50	<u>2</u>	

generates molecules with comparable Vina Energy but small atom numbers, leading to high LBE. For details, see Appendix. C.1.2.

Geometry. From Table. 6, conclusions can be drawn that (i) DECOMPDIFF generates overall the most realistic structures, according to the internal geometries, and TARGETDIFF is comparable. (ii) The molecule-protein clashes can usually be avoided by diffusion models, like DIFFBP, TARGETDIFF and DECOMPDIFF. However, in the auto-regressive models, only POCKET2MOL avoids clashes. The high frequency of clashes in auto-regressive methods can be explained as follows: These models first identify frontier amino acids or atoms within the molecule. During the placing of new atoms, incorrect binding site localization leads to an erroneous direction for the molecule’s auto-regressively growing path, causing it to extend inward towards the protein. For details, see Appendix. C.1.3.

Conclusion and Discussion. From Table. 7 and the previous discussion, we conclude that

- (i) The CNN-Based methods like LIGAN are still very competitive, which explains why such methods in the field of drug design still prevail in recent years [50, 51].
- (ii) TARGETDIFF achieves the best overall performance. In contrast, DECOMPDIFF as the version of TARGETDIFF that incorporates domain knowledge, D3FG and FLAG show degeneration in performance. This observation reveals that the current incorporation of physicochemical priors can hardly improve the quality of generated molecules. Effectively integrating domain knowledge to guide the model to generate structurally sound and biologically functional molecules remains a challenge. For example, atom clashes are very common in generated molecules, and integrating domain knowledge into general sampling techniques may help mitigate this issue [52, 53].
- (iii) Only POCKET2MOL as an auto-regressive method achieves competitive results, which we attribute to the following reasons: First, it utilizes chemical bonds to constrain atoms to grow orderly along chemical bonds rather than to grow based on distance to the pocket as in DIFFBP. Second, it simultaneously predicts the bond types and employs contrastive learning by sampling positive and negative instances of atom positions as real and fake bonds, which is not fully considered by FLAG, enhancing the model’s ability to perceive chemical bond patterns. Therefore, we believe that for autoregressive methods, enabling the model to successfully capture the patterns of chemical bonds is essential.

5.2 Extension on Subtasks

Setup. Lead optimization is to strengthen the function or property of the binding molecules by remodeling the existing partial 3D graph of molecules. We show the interaction analysis and chemical property in the main context and omit the interaction pattern analysis since maintaining the patterns is not necessary for lead optimization. From the discussion above, the data-driven methods can reach even better performance than the domain-knowledge-based ones, so we have not compared them here. Another reason is that for fragment-based methods, some tasks do not support the direct application of these methods, such as linker design. Besides, the voxelize-based methods are not easily extended to these tasks, and we regard the transferring of methods like LIGAN and 3DSBDD as future work. Hence, we here compare 5 methods that model atoms’ continuous positions with GNNs and have not employed domain knowledge. When training, since the number of training instances is smaller, we use the pretrained models on *de novo* generation and finetune the auto-regressive models with 1,000,000 iterations. For diffusion-based models with one-shot generation, we train them from scratch because the zero-center-of-mass [54] technique is shifted from employing protein geometric centers to using molecule context’s ones. For detailed results, please refer to Appendix. C.2.

Table 8: Results of subtasks for lead optimization.

Tasks	Methods	Metrics		Vina Score		Vina Min		Vina Dock				Chem. Prop.				Rank
		E_{vina}	IMP%	E_{vina}	IMP%	E_{vina}	IMP%	MPBG%	LBE	QED	LogP	SA	LPSK			
Linker	GRAPHBP	-	5.63	-0.97	12.43	-7.51	28.18	-7.36	0.3288	0.41	0.86	0.70	3.60	3.92		
	POCKET2MOL	-6.89	18.99	-7.19	25.04	-8.07	37.22	-3.85	0.3276	0.45	1.93	0.67	4.25	2.17		
	TARGETDIFF	-7.22	36.11	-7.60	41.31	-8.49	50.73	2.61	0.2993	0.39	1.63	0.61	4.02	2.33		
	DIFFSBDD	-5.64	11.06	-6.38	19.15	-7.88	34.97	-4.42	0.3110	0.42	1.14	0.66	4.10	3.33		
	DIFFBP	-6.27	35.49	-7.19	36.80	-8.74	54.33	6.60	0.3078	0.43	3.45	0.55	4.01	2.42		
Fragment	GRAPHBP	-5.54	4.86	-6.28	9.78	-7.16	16.21	-11.88	0.3749	0.54	0.87	0.66	4.66	3.00		
	POCKET2MOL	-6.87	22.78	-7.61	37.45	-8.33	54.05	-0.28	0.3310	0.46	1.02	0.63	4.07	1.75		
	TARGETDIFF	-6.06	24.56	-6.78	30.43	-7.96	42.00	-2.38	0.3003	0.45	1.43	0.58	4.28	2.67		
	DIFFSBDD	-4.64	19.14	-5.84	28.90	-7.66	37.18	-6.67	0.3076	0.47	0.73	0.58	4.39	3.42		
	DIFFBP	-4.51	22.31	-6.18	29.52	-7.90	45.70	-1.92	0.2952	0.46	2.24	0.49	4.30	3.33		
Side chain	GRAPHBP	-5.01	10.15	-5.43	11.46	-6.14	9.71	-11.05	0.4459	0.61	1.93	0.76	4.93	3.17		
	POCKET2MOL	-5.99	22.26	-6.56	33.29	-7.26	41.04	-4.34	0.3600	0.49	0.21	0.65	4.20	2.25		
	TARGETDIFF	-5.80	23.90	-6.50	35.81	-7.40	46.87	-2.55	0.3213	0.48	0.88	0.60	4.41	2.08		
	DIFFSBDD	-4.43	15.12	-5.99	30.23	-7.58	44.09	-9.38	0.3178	0.43	1.20	0.65	4.03	3.17		
	DIFFBP	-4.61	14.31	-5.73	24.29	-7.03	38.96	-7.38	0.3143	0.49	1.29	0.56	4.50	3.50		
Scaffold	GRAPHBP	-	0.00	-	0.06	-3.90	0.99	-50.62	0.3797	0.43	0.14	0.76	4.98	3.58		
	POCKET2MOL	-4.80	16.84	-5.71	23.08	-6.89	38.18	-8.07	0.3378	0.43	0.91	0.64	4.48	2.00		
	TARGETDIFF	-5.52	31.47	-5.86	34.39	-7.06	44.32	-6.22	0.3038	0.43	0.89	0.59	4.26	1.83		
	DIFFSBDD	-3.85	18.44	-4.90	22.12	-6.81	34.98	-10.23	0.2985	0.42	-0.13	0.53	4.29	3.33		
	DIFFBP	-2.09	13.89	-4.35	16.84	-6.46	32.43	-12.14	0.3025	0.43	3.37	0.56	4.44	3.42		

Conclusion and Discussion. From Table. 7 and the previous discussion, we conclude that

- (i) Overall, the performance gap among these methods in the lead optimization is not as pronounced compared to *de novo* generation. TARGETDIFF and POCKET2MOL still perform well. Notably, in the evaluation of initial stability, DIFFSBDD, DIFFBP, and GRAPHBP can optimize and complete the binding graph near the given partial molecular conformations, according to the columns of Vina Score and Vina Min. The applicability of GRAPHBP also reflects the Argument. (ii) in *de novo* geometry analysis: The failure of GraphBP mainly stems from the difficulty in locating the correct atoms for auto-regressive growth.
- (ii) In these tasks, scaffold hopping is the most challenging, as the improvement of generated molecules relative to the reference is minimal; Linker design is relatively the easiest. Notably, in scaffolding, there are still some methods that fail.

Additionally, there are several points that warrant further detailed design. For instance, in linker design, the fragments of the molecule that need to be connected may change orientation due to variations in the linker [18]; In side chain decoration, the protein’s side chains, which are the main components in interaction, should be generated together with the molecule’s side chains to achieve a stable conformation as the entire complex [55, 56].

5.3 Case study

Introduction. In order to verify whether the included methods can generalize to pharmaceutical targets and the applicability of CBGBench to real-world scenarios, we use the pretrained model in *de novo* generation, and apply them to two proteins belonging to the G-Protein-Coupled Receptor (GPCR) family: ARDB1 (beta-1 adrenergic receptor) and DRD3 (dopamine receptor D3). ARDB1 participates in the regulation of various physiological processes by responding to the neurotransmitter epinephrine (adrenaline) and norepinephrine, and drugs that selectively activate or block this receptor are used in the treatment of various cardiovascular conditions. For DRD3, it is primarily expressed in the brain, particularly in areas such as the limbic system and the ventral striatum with functions of mediating the effects of the neurotransmitter dopamine in the central nervous system.

Setup. On these targets, there are molecules reported active to them experimentally, we here randomly select 200 of them for each target and conduct two kinds of experiments. Firstly, we try to figure out if the model can generate binding molecules that have similar chemical distributions with the actives. We use extended connectivity fingerprint (ECFP) [57] to get the molecule fingerprint and employ t-SNE [58] for 2-dimensional visualization. Secondly, we aim to find out the distribution of Vina Docking Energy and LBE of the generated and the actives as the metrics for binding affinities. Seven methods except for voxelized-based ones (inflexible to extend to the framework) and DECOMPDIFF (requiring complex data-preprocessing for domain knowledge and differing from TARGETDIFF slightly) are tested on the two targets. Besides, we select 200 molecules randomly from GEOM-DRUG [59], as a randomized control sample set.

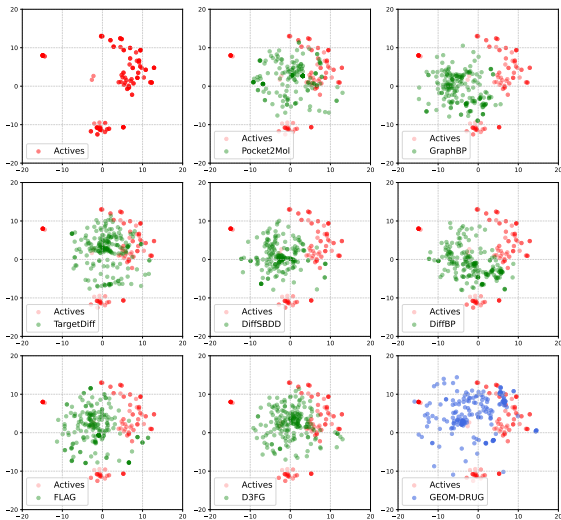
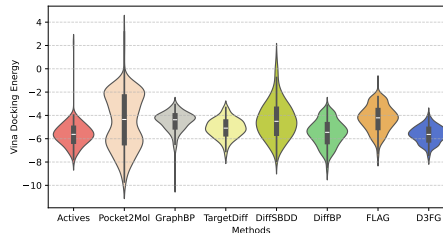
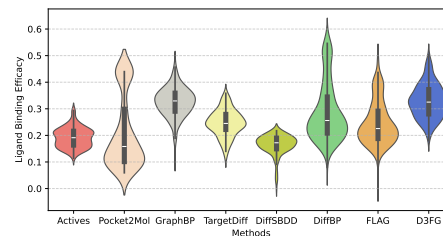


Figure 3: T-SNE visualization of chemical distributions of generated and active molecules on ADRB1.



(a) Distribution of Vina Dock Energy



(b) Distribution of LBE

Figure 4: Distribution of binding affinities.

Conclusion and Discussion. Figure 3 and Figure 4 gives the results on target ADRB1.

- (i) In Figure 3, we can see that POCKET2MOL, TARGETDIFF, and D3FG have better consistency in the chemical distribution of molecules, as evidenced by a greater degree of overlap with the actives. In addition, in comparison to randomly selected molecules in GEOM-DRUG, these models show different preferences in generating binding molecules since the clustering center in the chemical space differs.
- (ii) Figure 4 shows that in generating molecules based on the real-world target ADRB1, D3FG exhibits superior and stable performance. TARGETDIFF also perform well.

These conclusions are essentially consistent with the conclusion in Sec. 5.1, reflecting that the established evaluation protocols exhibit **strong consistency and generalizability on real-world target data**. Besides, it is worth noting that DIFFBP, FLAG, and POCKET2MOL can possibly generate molecules with small atom numbers and high LBE. This indicates that they have the potential to excel in lead discovery on ADRB1, as a good lead should possess good synthesizability and modifiability, smaller molecular weight, and stable binding conformations. For DRD3, please refer to Appendix. C.2.1 for details.

6 Conclusion and Limitation

In this paper, we propose CBGBench. It first unifies the tasks of SBDD and lead optimization into a 3D-graph completion problem as a fill-in-the-blank 3D binding graph and introduces four additional lead optimization tasks. Then, it comprehensively categorizes existing methods based on certain criteria, modularizes these methods based on the categorization, and integrates them into a unified codebase for fair comparison. Additionally, it extends existing evaluation protocols by incorporating aspects such as interaction pattern, ligand binding efficacy, and protein-atom clash ratio as important evaluation metrics, addressing the issue of incomplete and diverse evaluation process. Finally, through extensive experiments and by extending the pretrained models to real targets for molecule generation, we derive a series of insightful conclusions and identify future research directions.

However, there are certain limitations. Firstly, this codebase is primarily based on GNNs, so some voxelized-grid-based methods that require the use of CNNs have not been included. Engineering the integration of these types of methods will be a focus of our future work. Secondly, due to the inability to use wet lab experiments for validation, many of the metrics are obtained through computational chemistry methods. These computational functions are often considered unable to accurately reflect the chemical properties of molecules, such as the calculated SA (Synthetic Accessibility) and AutoDock Vina energy. Therefore, how to utilize AI to assist in accurate metric calculation will also be a key focus of our future research.

References

- [1] John M. Jumper, Richard Evans, Alexander Pritzel, Tim Green, Michael Figurnov, Olaf Ronneberger, Kathryn Tunyasuvunakool, Russ Bates, Augustin Žídek, Anna Potapenko, Alex Bridgland, Clemens Meyer, Simon A A Kohl, Andy Ballard, Andrew Cowie, Bernardino Romera-Paredes, Stanislav Nikolov, Rishub Jain, Jonas Adler, Trevor Back, Stig Petersen, David Reiman, Ellen Clancy, Michal Zielinski, Martin Steinegger, Michalina Pacholska, Tamas Berghammer, Sebastian Bodenstein, David Silver, Oriol Vinyals, Andrew W. Senior, Koray Kavukcuoglu, Pushmeet Kohli, and Demis Hassabis. Highly accurate protein structure prediction with alphafold. *Nature*, 596:583 – 589, 2021.
- [2] Joseph L Watson, David Juergens, Nathaniel R. Bennett, Brian L. Trippe, Jason Yim, Helen E. Eisenach, Woody Ahern, Andrew J. Borst, Robert J. Ragotte, Lukas F. Milles, Basile I. M. Wicky, Nikita Hanikel, Samuel J. Pellock, Alexis Courbet, William Sheffler, Jue Wang, Preetham Venkatesh, Isaac Sappington, Susana Vázquez Torres, Anna Lauko, Valentin De Bortoli, Emile Mathieu, Sergey Ovchinnikov, Regina Barzilay, T. Jaakkola, Frank DiMaio, Minkyung Baek, and David Baker. De novo design of protein structure and function with rfdiffusion. *Nature*, 620:1089 – 1100, 2023.
- [3] Rohith Krishna, Jue Wang, Woody Ahern, Pascal Sturmfels, Preetham Venkatesh, Indrek Kalvet, Gyu Rie Lee, Felix S Morey-Burrows, Ivan V. Anishchenko, Ian R. Humphreys, Ryan McHugh, Dionne Vafeados, Xinting Li, George A. Sutherland, Andrew Hitchcock, C Neil Hunter, Alex Kang, Evans Brackenbrough, Asim K. Bera, Minkyung Baek, Frank DiMaio, and David Baker. Generalized biomolecular modeling and design with rosettafold all-atom. *bioRxiv*, 2023.
- [4] Jonathan Ho, Ajay Jain, and P. Abbeel. Denoising diffusion probabilistic models. *ArXiv*, abs/2006.11239, 2020.
- [5] Yaron Lipman, Ricky T. Q. Chen, Heli Ben-Hamu, Maximilian Nickel, and Matt Le. Flow matching for generative modeling. *ArXiv*, abs/2210.02747, 2022.
- [6] Yang Song, Jascha Narain Sohl-Dickstein, Diederik P. Kingma, Abhishek Kumar, Stefano Ermon, and Ben Poole. Score-based generative modeling through stochastic differential equations. *ArXiv*, abs/2011.13456, 2020.
- [7] Meng Liu, Youzhi Luo, Kanji Uchino, Koji Maruhashi, and Shuiwang Ji. Generating 3d molecules for target protein binding. *ArXiv*, abs/2204.09410, 2022.
- [8] Paul G. Francoeur, Tomohide Masuda, Jocelyn Sunseri, Andrew Jia, Richard B. Iovanisci, Ian Snyder, and David Ryan Koes. 3d convolutional neural networks and a crossdocked dataset for structure-based drug design. *Journal of chemical information and modeling*, 2020.
- [9] Xingang Peng, Shitong Luo, Jiaqi Guan, Qi Xie, Jian Peng, and Jianzhu Ma. Pocket2mol: Efficient molecular sampling based on 3d protein pockets. In *International Conference on Machine Learning*, 2022.
- [10] Shitong Luo, Jiaqi Guan, Jianzhu Ma, and Jian Peng. A 3d generative model for structure-based drug design, 2022.
- [11] Haitao Lin, Yufei Huang, Meng Liu, Xuan Cindy Li, Shuiwang Ji, and Stan Z. Li. Diffbp: Generative diffusion of 3d molecules for target protein binding. *ArXiv*, abs/2211.11214, 2022.
- [12] Andrew T. McNutt, Paul G. Francoeur, Rishal Aggarwal, Tomohide Masuda, Rocco Meli, Matthew Ragoza, Jocelyn Sunseri, and David Ryan Koes. Gnina 1.0: molecular docking with deep learning. *Journal of Cheminformatics*, 13, 2021.
- [13] Oleg Trott and Arthur J. Olson. Autodock vina: Improving the speed and accuracy of docking with a new scoring function, efficient optimization, and multithreading. *Journal of Computational Chemistry*, 31, 2009.
- [14] Jiaqi Guan, Wesley Wei Qian, Xingang Peng, Yufeng Su, Jian Peng, and Jianzhu Ma. 3d equivariant diffusion for target-aware molecule generation and affinity prediction. In *The Eleventh International Conference on Learning Representations*, 2023.
- [15] Victor Garcia Satorras, Emiel Hooeboom, and Max Welling. E(n) equivariant graph neural networks, 2022.
- [16] Bowen Jing, Stephan Eismann, Patricia Suriana, Raphael J. L. Townshend, and Ron O. Dror. Learning from protein structure with geometric vector perceptrons. *ArXiv*, abs/2009.01411, 2020.

- [17] Ilia Igashov, Hannes Stärk, Clément Vignac, Victor Garcia Satorras, Pascal Frossard, Max Welling, Michael M. Bronstein, and Bruno E. Correia. Equivariant 3d-conditional diffusion models for molecular linker design. *ArXiv*, abs/2210.05274, 2022.
- [18] Jiaqi Guan, Xingang Peng, Peiqi Jiang, Yunan Luo, Jian Peng, and Jianzhu Ma. Linkernet: Fragment poses and linker co-design with 3d equivariant diffusion. In *Neural Information Processing Systems*, 2023.
- [19] Tomohide Masuda, Matthew Ragoza, and David Ryan Koes. Generating 3d molecular structures conditional on a receptor binding site with deep generative models. *ArXiv*, abs/2010.14442, 2020.
- [20] Diederik P Kingma and Max Welling. Auto-encoding variational bayes, 2022.
- [21] Arne Schneuing, Yuanqi Du, Charles Harris, Arian R. Jamasb, Ilia Igashov, Weitao Du, Tom L. Blundell, Pietro Li'o, Carla P. Gomes, Max Welling, Michael M. Bronstein, and Bruno E. Correia. Structure-based drug design with equivariant diffusion models. *ArXiv*, abs/2210.13695, 2022.
- [22] Haitao Lin, Yufei Huang, Haotian Zhang, Lirong Wu, Siyuan Li, Zhiyuan Chen, and Stan Z. Li. Functional-group-based diffusion for pocket-specific molecule generation and elaboration. *ArXiv*, abs/2306.13769, 2023.
- [23] ZAI XI ZHANG, Yaosen Min, Shuxin Zheng, and Qi Liu. Molecule generation for target protein binding with structural motifs. In *The Eleventh International Conference on Learning Representations*, 2023.
- [24] Jiaqi Guan, Xiangxin Zhou, Yuwei Yang, Yu Bao, Jian Peng, Jianzhu Ma, Qiang Liu, Liang Wang, and Quanquan Gu. DecompDiff: Diffusion models with decomposed priors for structure-based drug design. In Andreas Krause, Emma Brunskill, Kyunghyun Cho, Barbara Engelhardt, Sivan Sabato, and Jonathan Scarlett, editors, *Proceedings of the 40th International Conference on Machine Learning*, volume 202 of *Proceedings of Machine Learning Research*, pages 11827–11846. PMLR, 23–29 Jul 2023.
- [25] Odin Zhang, Haitao Lin, Hui Zhang, Huifeng Zhao, Yufei Huang, Yuansheng Huang, Dejun Jiang, Chang-yu Hsieh, Peichen Pan, and Tingjun Hou. Deep lead optimization: Leveraging generative ai for structural modification. *arXiv preprint arXiv:2404.19230*, 2024.
- [26] Dylan Grenier, Solène Audebert, Jordane Preto, Jean-François Guichou, and Isabelle Krimm. Linkers in fragment-based drug design: an overview of the literature. *Expert Opinion on Drug Discovery*, 18(9):987–1009, 2023.
- [27] Daniel A Erlanson, Stephen W Fesik, Roderick E Hubbard, Wolfgang Jahnke, and Harren Jhoti. Twenty years on: the impact of fragments on drug discovery. *Nature reviews Drug discovery*, 15(9):605–619, 2016.
- [28] Alexandre Bancet, Claire Rängeval, Thierry Lomberget, Marc Le Borgne, Jean-François Guichou, and Isabelle Krimm. Fragment linking strategies for structure-based drug design. *Journal of Medicinal Chemistry*, 63(20):11420–11435, 2020.
- [29] Alvinemsp14W Hung, H emsp14Leonardo Silvestre, Shijun Wen, Alessio Ciulli, Tomemsp14L Blundell, and Chris Abell. Application of fragment growing and fragment linking to the discovery of inhibitors of mycobacterium tuberculosis pantothenate synthetase. *Angewandte Chemie International Edition*, 48(45):8452–8456, 2009.
- [30] Jiaqi Guan, Xiangxin Zhou, Yuwei Yang, Yu Bao, Jian Peng, Jianzhu Ma, Qiang Liu, Liang Wang, and Quanquan Gu. Decompdiff: diffusion models with decomposed priors for structure-based drug design. *arXiv preprint arXiv:2403.07902*, 2024.
- [31] Guy W Bemis and Mark A Murcko. The properties of known drugs. 1. molecular frameworks. *Journal of medicinal chemistry*, 39(15):2887–2893, 1996.
- [32] Gisbert Schneider, Werner Neidhart, Thomas Giller, and Gerard Schmid. “scaffold-hopping” by topological pharmacophore search: a contribution to virtual screening. *Angewandte Chemie International Edition*, 38(19):2894–2896, 1999.
- [33] Hongmao Sun, Gregory Tawa, and Anders Wallqvist. Classification of scaffold-hopping approaches. *Drug discovery today*, 17(7-8):310–324, 2012.

- [34] Elena S. Salmina, Norbert Haider, and Igor V. Tetko. Extended functional groups (efg): An efficient set for chemical characterization and structure-activity relationship studies of chemical compounds. *Molecules*, 21, 2015.
- [35] Arup K. Ghose, Vellarkad N. Viswanadhan, and John J. Wendoloski. A knowledge-based approach in designing combinatorial or medicinal chemistry libraries for drug discovery. 1. a qualitative and quantitative characterization of known drug databases. *Journal of combinatorial chemistry*, 1 1:55–68, 1999.
- [36] Cele Abad-Zapatero and James T Metz. Ligand efficiency indices as guideposts for drug discovery. *Drug discovery today*, 10(7):464–469, 2005.
- [37] Andrew L Hopkins, György M Keserü, Paul D Leeson, David C Rees, and Charles H Reynolds. The role of ligand efficiency metrics in drug discovery. *Nature reviews Drug discovery*, 13(2):105–121, 2014.
- [38] Odin Zhang, Jintu Zhang, Jieyu Jin, Xujun Zhang, Renling Hu, Chao Shen, Hanqun Cao, Hongyan Du, Yu Kang, Yafeng Deng, Furui Liu, Guangyong Chen, Chang-Yu Hsieh, and Tingjun Hou. Resgen is a pocket-aware 3d molecular generation model based on parallel multiscale modelling. *Nature Machine Intelligence*, 5:1020 – 1030, 2023.
- [39] Melissa F. Adasme, Katja L Linnemann, Sarah Naomi Bolz, Florian Kaiser, Sebastian Salentin, V. Joachim Haupt, and Michael Schroeder. Plip 2021: expanding the scope of the protein–ligand interaction profiler to dna and rna. *Nucleic Acids Research*, 49:W530 – W534, 2021.
- [40] Jia li Zuo, Changqian Yu, Nong Sang, and Changxin Gao. Plip: Language-image pre-training for person representation learning. *ArXiv*, abs/2305.08386, 2023.
- [41] Sebastian Salentin, Sven Schreiber, V. Joachim Haupt, Melissa F. Adasme, and Michael Schroeder. Plip: fully automated protein–ligand interaction profiler. *Nucleic Acids Research*, 43:W443 – W447, 2015.
- [42] Bowen Jing, Gabriele Corso, Jeffrey Chang, Regina Barzilay, and T. Jaakkola. Torsional diffusion for molecular conformer generation. *ArXiv*, abs/2206.01729, 2022.
- [43] Kirk Swanson, Jake Williams, and Eric Jonas. Von mises mixture distributions for molecular conformation generation, 2023.
- [44] Srinivas Ramachandran, Pradeep Kota, Feng Ding, and Nikolay V. Dokholyan. Automated minimization of steric clashes in protein structures. *Proteins: Structure*, 79, 2011.
- [45] Milton Friedman. A comparison of alternative tests of significance for the problem of m rankings. *Annals of Mathematical Statistics*, 11:86–92, 1940.
- [46] Milton Friedman. The use of ranks to avoid the assumption of normality implicit in the analysis of variance. *Journal of the American Statistical Association*, 32:675–701, 1937.
- [47] Yidong Wang, Hao Chen, Yue Fan, Wangbin Sun, Ran Tao, Wenxin Hou, Renjie Wang, Linyi Yang, Zhi Zhou, Lan-Zhe Guo, Heli Qi, Zhen Wu, Yu-Feng Li, Satoshi Nakamura, Weirong Ye, Marios Savvides, Bhiksha Raj, Takahiro Shinozaki, Bernt Schiele, Jindong Wang, Xingxu Xie, and Yue Zhang. Usb: A unified semi-supervised learning benchmark. *ArXiv*, abs/2208.07204, 2022.
- [48] Petar Veličković, Guillem Cucurull, Arantxa Casanova, Adriana Romero, Pietro Liò, and Yoshua Bengio. Graph attention networks, 2018.
- [49] Miltiadis Kofinas, Naveen Shankar Nagaraja, and Efstratios Gavves. Roto-translated local coordinate frames for interacting dynamical systems, 2022.
- [50] Pedro O. Pinheiro, Joshua Rackers, Joseph Kleinhenz, Michael Maser, Omar Mahmood, Andrew Martin Watkins, Stephen Ra, Vishnu Sresht, and Saeed Saremi. 3d molecule generation by denoising voxel grids, 2024.
- [51] Pedro O. Pinheiro, Arian Jamasb, Omar Mahmood, Vishnu Sresht, and Saeed Saremi. Structure-based drug design by denoising voxel grids, 2024.
- [52] Lei Huang, Tingyang Xu, Yang Yu, Peilin Zhao, Xingjian Chen, Jing Han, Zhi Xie, Hailong Li, Wenge Zhong, Ka-Chun Wong, and Hengtong Zhang. A dual diffusion model enables 3d molecule generation and lead optimization based on target pockets. *Nature Communications*, 15, 2024.

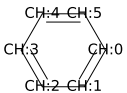
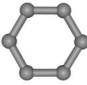
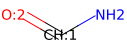
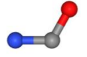
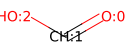
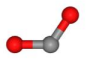
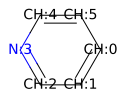
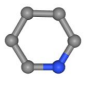
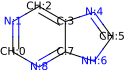
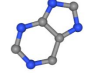

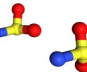
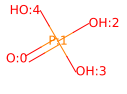

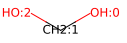
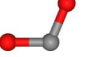

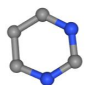
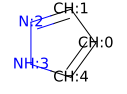
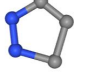
- [53] Keir Adams and Connor W. Coley. Equivariant shape-conditioned generation of 3d molecules for ligand-based drug design. In *The Eleventh International Conference on Learning Representations*, 2023.
- [54] Victor Garcia Satorras, Emiel Hoogeboom, Fabian B. Fuchs, Ingmar Posner, and Max Welling. E(n) equivariant normalizing flows. In *Neural Information Processing Systems*, 2021.
- [55] Shitong Luo, Yufeng Su, Zuofan Wu, Chenpeng Su, Jian Peng, and Jianzhu Ma. Rotamer density estimator is an unsupervised learner of the effect of mutations on protein-protein interaction. In *The Eleventh International Conference on Learning Representations*, 2023.
- [56] Yufei Huang, Odin Zhang, Lirong Wu, Cheng Tan, Haitao Lin, Zhangyang Gao, Siyuan Li, and Stan. Z. Li. Re-dock: Towards flexible and realistic molecular docking with diffusion bridge, 2024.
- [57] David Rogers and Mathew Hahn. Extended-connectivity fingerprints. *Journal of chemical information and modeling*, 50 5:742–54, 2010.
- [58] Laurens van der Maaten and Geoffrey E. Hinton. Visualizing data using t-sne. *Journal of Machine Learning Research*, 9:2579–2605, 2008.
- [59] Simon Axelrod and Rafael Gómez-Bombarelli. Geom, energy-annotated molecular conformations for property prediction and molecular generation. *Scientific Data*, 9(1):185, 2022.
- [60] RDKit: Open-source cheminformatics. <http://www.rdkit.org>. [Online; accessed 11-April-2013].
- [61] Open Babel development team. Open babel.

A Supplementary Evaluation Details

A.1 Included Functional Groups

Here we show the functional groups included in this paper, in which we follow D3FG and give a demonstration of them in Table. 9.

Table 9: The included functional groups in CBGBench. ‘T’ is the occurrence times of the functional group in the datasets (100,000 ligands). ‘A,B,C’ are the framing node index.

Smiles	2D graph	3D structures	A	B	C	T
<chem>c1ccccc1</chem>			1	0	2	131148
<chem>NC=O</chem>			1	0	2	49023
<chem>O=CO</chem>			1	0	2	39863
<chem>c1ccncc1</chem>			3	2	4	15115
<chem>c1ncc2nc[nH]c2n1</chem>			7	3	6	11369
<chem>NS(=O)=O</chem>			1	0	2	10121
<chem>O=P(O)(O)O</chem>			1	0	2	7451
<chem>OCO</chem>			1	0	2	6405
<chem>c1cncnc1</chem>			3	2	4	5965
<chem>c1cn[nH]c1</chem>			2	3	1	5404

Smiles	2D graph	3D structures	A	B	C	T
<chem>O=P(O)O</chem>			0	1	center(2,3)	5271
<chem>c1ccc2ccccc2c1</chem>			3	2	4	4742
<chem>c1ccsc1</chem>			3	2	4	4334
<chem>N=CN</chem>			1	0	2	4315
<chem>NC(N)=O</chem>			2	1	3	4167
<chem>O=c1cc[nH]c(=O)[nH]1</chem>			7	1	5	4145
<chem>c1ccc2ncccc2c1</chem>			3	2	4	3519
<chem>c1cscn1</chem>			2	3	1	3466
<chem>c1ccc2[nH]cnc2c1</chem>			5	4	6	3462
<chem>c1c[nH]cn1</chem>			3	2	4	2964
<chem>O=[N+][O-]</chem>			1	0	2	2702
<chem>O=CNO</chem>			1	0	2	2477
<chem>NC(=O)O</chem>			1	0	2	2438
<chem>O=S=O</chem>			1	0	2	2375
<chem>c1ccc2[nH]ccc2c1</chem>			3	4	2	2301

A.2 LBE Analysis

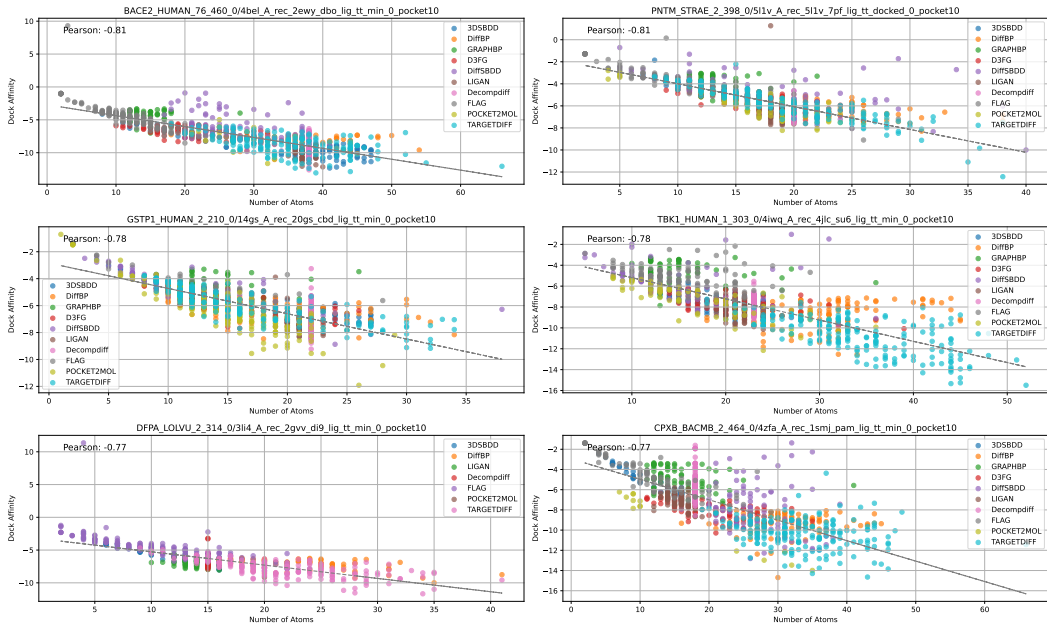


Figure 5: A demonstration of how the molecule size affects the binding energy. The 6 pockets that are most linear-correlated with atom number.

A.3 Metric Calculation

The metric of MPBG can be written as $MPBG_j = \text{Mean}_i(\frac{E_{i, \text{gen}} - E_{\text{ref}}}{E_{\text{ref}}} \times 100\%)$, in which i is the indicator of the generated molecules in a single protein and $\text{Mean}_i(\cdot)$ calculates average along indicator i , with $MPBG = \text{Mean}_j(MPBG_j)$. The MPBG is a per-pocket metric that is calculated within a single pocket, which differs from other averaging metrics.

For chemical property calculation, we use functions in RDKit [60], and note that the SA is the normalized one employed in the previous studies.

For interaction pattern analysis, we employ PLIP, which considers 7 kinds of interaction types including ‘hydrophobic interactions’, ‘hydrogen bonds’, ‘water bridges’, ‘ π -stacks’, ‘ π -cation interactions’, ‘halogen bonds’ and ‘metal complexes’.

For MAE metrics which are related to the molecule sizes, the generative model tends to achieve higher scores when the atom number is close to that of the reference. We suppose it is reasonable, considering that the size of the molecule itself is determined by factors such as the size and shape of the pocket, and these characteristics should be captured by the models.

B Codebase Structure

In this section, we provide an overview of the codebase structure of CBGBench, where four abstract layers are adopted. The layers include the core layer, algorithm layer, chemistry layer, and API layer in the bottom-up direction as shown in Fig. 6. This codebase is licensed under the Apache License, Version 2.0. It provides a robust and flexible framework for building and evaluating graph neural network models for structure-based drug design and lead optimization.

Core Layer. In the core layer, we implement the commonly used core functions for training and sampling CBG algorithms. Besides, the code regarding datasets, data loaders, and basic modules used in CBGBench is also provided in the core layer.

Algorithm Layer. In the algorithm layer, we first implement the base class for CBG algorithms, where we initialize the datasets, data loaders, and basic modules from the core layer. We modularize

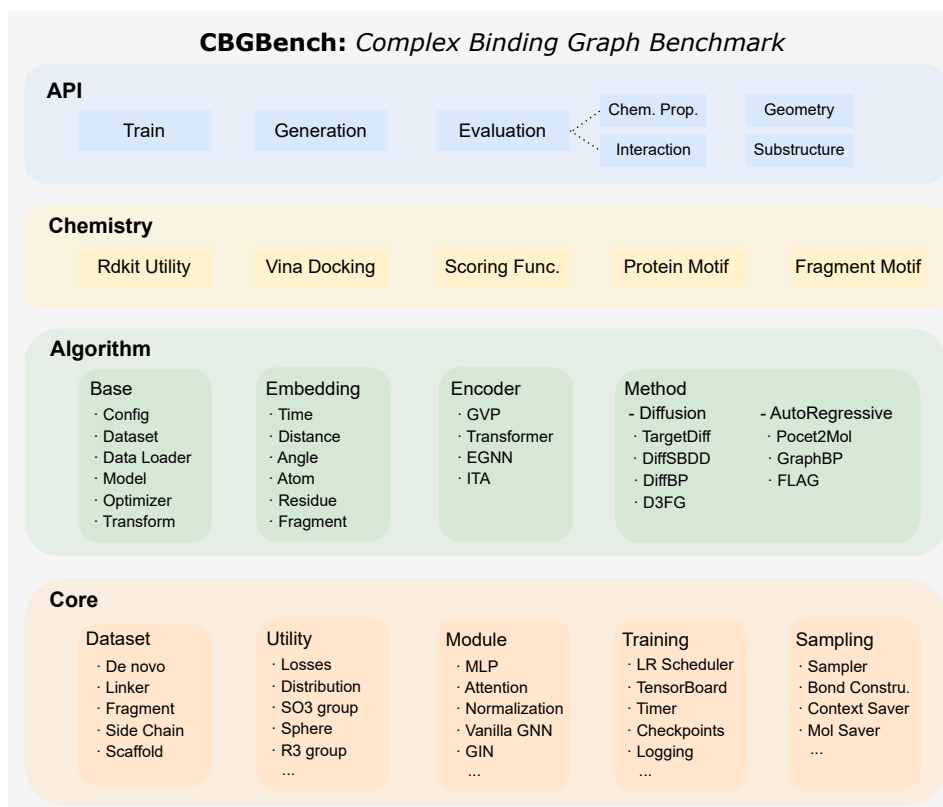


Figure 6: Structure of CBGBench Codebase, consisting of 4 layers. The core layer provides the common functions, datasets, and modules for CBG methods. The algorithm layer mainly implements the prevailing CBG algorithms. The Chemistry layer is used for data preprocessing and evaluation.

each method, first using embedding layers to project the input into high-dimensional space, and then employing different 3D equivariant GNNs to construct the algorithm, including Diffusion-based and Auto-regressive-based ones. We further abstract the algorithms, enabling better code reuse and making it easier to implement new algorithms. The voxel-based methods are not included because our framework is mostly based on EGNNs, which will be added to the codebase as future work, and DecompDiff requires different data preprocessing. Based on this, we support 7 core CBG algorithms. More algorithms are expected to be added through continued extension.

Chemistry Layer. The chemistry layer is mostly built with post-processing utilities and evaluators such as atom type, bond angle, and docking modules. Besides, several prior decomposition functions are used as molecule parsers, and the molecule and protein fragment motifs serve as prior knowledge.

API Layer. We wrap the core functions and algorithms in CBGBench in the API layer as a public Python package. It is friendly for users from different backgrounds who want to employ CGB algorithms in new applications. Training and sampling can be done in only a few lines of code. In addition, we provide the configuration files of all algorithms supported in CBGBench with detailed parameter settings, allowing the reproduction of the results.

C Experimental Result Details

C.1 Denovo Generation

C.1.1 Substructure

Table. 10 gives the generated molecules’ atom distribution in detail. It shows DIFFBP and GRAPHBP tend to generate more C atoms and have a low probability of generating uncommon atoms. In contrast, D3FG and FLAG, which directly use a motif library, have a higher probability of generating these uncommon atoms. Table. 11 gives the generated molecules’ ring distribution in detail. DIFFBP and DIFFSBDD perform poorly due to significant inconsistencies in generating large complex fragments. For example, they also generate a large number of unreasonable triangular and tetrahedral rings. Similarly, these methods also fall short in generating complex functional groups, as shown in Table. 12. This leads to their subpar performance in substructure generation.

Table 10: Distribution of different atom types across different methods.

Method	C	N	O	F	P	S	Cl
REF.	0.6715	0.1170	0.1696	0.0131	0.0111	0.0112	0.0064
LIGAN	0.6477	0.0775	0.2492	0.0005	0.0224	0.0019	0.0008
3DSBDD	0.6941	0.1311	0.1651	0.0025	0.0063	0.0010	0.0000
GRAPHBP	0.8610	0.0397	0.0868	0.0036	0.0040	0.0039	0.0010
POCKET2MOL	0.7623	0.0855	0.1413	0.0025	0.0044	0.0027	0.0013
TARGETDIFF	0.6935	0.0896	0.1924	0.0110	0.0059	0.0052	0.0025
DIFFSBDD	0.7000	0.1154	0.1611	0.0081	0.0017	0.0093	0.0031
DIFFBP	0.9178	0.0030	0.0792	0.0000	0.0000	0.0000	0.0000
FLAG	0.5585	0.1341	0.2077	0.0265	0.0312	0.0347	0.0074
D3FG	0.7336	0.1158	0.1286	0.0056	0.0035	0.0088	0.0040
DECOMPDIFF	0.6762	0.0978	0.1927	0.0064	0.0149	0.0088	0.0033

Table 11: Distribution of different ring sizes across various methods.

Method	3	4	5	6	7	8
REF.	0.0130	0.0020	0.2855	0.6894	0.0098	0.0003
LIGAN	0.2238	0.0698	0.2599	0.4049	0.0171	0.0096
3DSBDD	0.2970	0.0007	0.1538	0.5114	0.0181	0.0116
GRAPHBP	0.0000	0.2429	0.1922	0.1765	0.1533	0.1113
POCKET2MOL	0.0000	0.1585	0.1822	0.4373	0.1410	0.0478
TARGETDIFF	0.0000	0.0188	0.2856	0.4918	0.1209	0.0298
DIFFSBDD	0.2842	0.0330	0.2818	0.2854	0.0718	0.0193
DIFFBP	0.0000	0.2195	0.2371	0.2215	0.1417	0.0707
FLAG	0.0000	0.0682	0.2716	0.5228	0.0996	0.0231
D3FG	0.0000	0.0201	0.2477	0.5966	0.0756	0.0283
DECOMPDIFF	0.0302	0.0378	0.3407	0.4386	0.1137	0.0196

Table 12: Distribution of the top ten functional groups across different methods.

Functional Group	REF.	LIGAN	3DSBDD	GRAPHBP	POCKET2MOL	TARGETDIFF	DIFFSBDD	DIFFBP	FLAG	D3FG	DECOMPDIFF
c1c1c1c1c1	0.3920	0.3464	0.3109	0.0133	0.3794	0.2729	0.0073	0.1962	0.2223	0.3002	0.3173
NC=O	0.1465	0.0998	0.1488	0.1330	0.1098	0.1520	0.1985	0.0108	0.1880	0.1597	0.1660
O=CO	0.1192	0.1549	0.1219	0.1888	0.2906	0.3085	0.5787	0.4440	0.1736	0.2078	0.2125
c1c1c1c1	0.0452	0.0546	0.0769	0.0000	0.0305	0.0427	0.0194	0.0010	0.0365	0.0323	0.0527
c1nc2nc[nH]c2n1	0.0340	0.1028	0.0090	0.0000	0.0000	0.0001	0.0000	0.0000	0.0009	0.0114	0.0094
NS(=O)=O	0.0303	0.0127	0.0000	0.0000	0.0000	0.0000	0.0073	0.0000	0.0000	0.0000	0.0057
O=P(O)(O)O	0.0223	0.0490	0.0814	0.0000	0.0150	0.0241	0.0000	0.0000	0.0014	0.0212	0.0418
OCO	0.0191	0.0897	0.0915	0.6064	0.0964	0.0855	0.0145	0.3289	0.2471	0.0751	0.0443
c1cnc1	0.0178	0.0197	0.0148	0.0000	0.0030	0.0069	0.0000	0.0000	0.0135	0.0410	0.0134
c1cn[nH]c1	0.0162	0.0000	0.0291	0.0000	0.0000	0.0065	0.0000	0.0000	0.0014	0.0000	0.0128

C.1.2 Interaction

PLIP Interaction Pattern. Table. 13 and 14 provide detailed interaction pattern analysis. Most models captured good interaction patterns, generating a substantial amount of hydrophobic and hydrogen interactions. DiffSBDD excessively generated hydrophobic interactions. Additionally, for interactions such as π -stacking, π -cation, and halogen interactions, which do not exist in the reference molecules, the models could probabilistically generate molecules capable of producing such interactions with the protein.

C.1.3 Geometry

Here we give detailed bond length and bond angle distribution of the evaluated method’s generated molecules and the reference, in Table. 15 and 16. It shows that the

Table 13: Frequency of interaction type.

Method	hydrophobic	hydrogen	water bridge	π -stacks	π -cation	halogen	metal
REF.	3.0000	3.0000	0.0000	0.0000	0.0000	0.0000	0.0000
LIGAN	3.1354	3.5078	0.0000	0.1045	0.0441	0.0034	0.0000
3DSBDD	3.1237	3.0853	0.0000	0.1405	0.0434	0.0053	0.0000
GRAPHBP	5.2008	0.8039	0.0000	0.0007	0.0046	0.0060	0.0000
POCKET2MOL	4.9366	1.8840	0.0000	0.0176	0.0081	0.0045	0.0000
TARGETDIFF	4.2444	3.5309	0.0000	0.1159	0.0377	0.0384	0.0000
DIFFSBDD	3.9009	3.3202	0.0000	0.0986	0.0338	0.0279	0.0000
DIFFBP	4.1027	1.4830	0.0000	0.0213	0.0039	0.0000	0.0000
FLAG	1.9319	2.1490	0.0000	0.0134	0.0185	0.0528	0.0000
D3FG	4.3149	2.4718	0.0000	0.0607	0.0260	0.0200	0.0000
DECOMPDIFF	3.9284	3.4531	0.0000	0.1177	0.0436	0.0290	0.0000

Table 14: Distribution of interaction type.

Method	hydrophobic	hydrogen	water bridge	π -stacks	π -cation	halogen	metal
REF.	0.5000	0.5000	0.0000	0.0000	0.0000	0.0000	0.0000
LIGAN	0.4614	0.5162	0.0000	0.0154	0.0065	0.0005	0.0000
3DSBDD	0.4882	0.4822	0.0000	0.0220	0.0068	0.0008	0.0000
GRAPHBP	0.8645	0.1336	0.0000	0.0001	0.0008	0.0010	0.0000
POCKET2MOL	0.7206	0.2750	0.0000	0.0026	0.0012	0.0007	0.0000
TARGETDIFF	0.5327	0.4432	0.0000	0.0146	0.0047	0.0048	0.0000
DIFFSBDD	0.5285	0.4498	0.0000	0.0134	0.0046	0.0038	0.0000
DIFFBP	0.6579	0.3398	0.0000	0.0020	0.0004	0.0000	0.0000
FLAG	0.4638	0.5159	0.0000	0.0032	0.0045	0.0127	0.0000
D3FG	0.6259	0.3586	0.0000	0.0088	0.0038	0.0029	0.0000
DECOMPDIFF	0.5188	0.4560	0.0000	0.0155	0.0058	0.0038	0.0000

Table 15: JSD Bond Length Comparisons across different methods.

METHOD	C-C	C-N	C-O	C=C	C=N	C=O
LIGAN	0.4986	0.4146	0.4560	0.4807	0.4776	0.4595
3DSBDD	0.2090	0.4258	0.5478	0.5170	0.6701	0.6448
GRAPHBP	0.5038	0.4231	0.4973	0.6235	0.4629	0.5986
POCKET2MOL	0.5667	0.5698	0.5433	0.4787	0.5989	0.5025
TARGETDIFF	0.3101	0.2490	0.3072	0.1715	0.1944	0.3629
DIFFSBDD	0.3841	0.3708	0.3291	0.3043	0.3473	0.3647
DIFFBP	0.5704	0.5256	0.5090	0.6161	0.6314	0.5296
FLAG	0.3460	0.3770	0.4433	0.4872	0.4464	0.4292
D3GF	0.4244	0.3227	0.3895	0.3860	0.3570	0.3566
DECOMPDIFF	0.2562	0.2007	0.2361	0.2590	0.2844	0.3091

Table 16: JSD Bond Angle Comparisons across different methods.

JSD _{BA}	LIGAN	3DSBDD	GRAPHBP	POCKET2MOL	TARGETDIFF	DIFFSBDD	DIFFBP	FLAG	D3GF	DECOMPDIFF
C#C-C	0.6704	0.4838	0.7507	0.6477	0.6845	0.6788	0.7204	0.4591	0.7027	0.8174
C-C#N	0.8151	0.2980	0.8326	0.5830	0.7437	0.7388	0.7928	0.3461	0.7120	0.7254
C-C-C	0.5260	0.2189	0.5015	0.4663	0.2955	0.3825	0.5234	0.3439	0.3703	0.2306
C-C-N	0.5102	0.2934	0.4975	0.4790	0.2738	0.4265	0.5189	0.3650	0.3592	0.1987
C-C-O	0.5198	0.3279	0.5216	0.5078	0.3335	0.3930	0.5327	0.3710	0.4021	0.2124
C-C=C	0.4657	0.2701	0.4430	0.2826	0.1815	0.3163	0.5047	0.2830	0.2706	0.2215
C-C=N	0.4441	0.4159	0.4376	0.3507	0.2075	0.3185	0.5171	0.3353	0.3205	0.2094
C-N-C	0.5209	0.3176	0.4586	0.3981	0.2915	0.4168	0.5378	0.4237	0.3597	0.1952
C-N-N	0.5889	0.2847	0.5403	0.4997	0.2626	0.4022	0.6005	0.4161	0.3505	0.2825
C-N-O	0.7019	0.4996	0.6338	0.6173	0.3263	0.4653	0.7070	0.5560	0.4943	0.3120
C-N=C	0.3646	0.4011	0.5133	0.3728	0.3105	0.3191	0.4433	0.4085	0.4517	0.3467
C-N=N	0.3597	0.6214	0.7639	0.7062	0.4400	0.4212	0.8326	0.7023	0.7380	0.3917
C-O-C	0.5111	0.4259	0.4872	0.4204	0.2865	0.3786	0.5478	0.4606	0.3765	0.1882
C-O-N	0.7893	0.3465	0.6637	0.6140	0.4312	0.5485	0.7520	0.6257	0.4988	0.4064
C=C-N	0.4580	0.4140	0.5415	0.3732	0.2359	0.3223	0.4075	0.3361	0.3226	0.2574
C=C=C	0.7593	0.6866	0.7793	0.7373	0.7445	0.7549	0.7752	0.7419	0.7603	0.7703
N#C-C	0.8151	0.2980	0.8326	0.5830	0.7437	0.7388	0.7928	0.3461	0.7120	0.7254
N-C-N	0.5157	0.3795	0.4179	0.5544	0.3058	0.4409	0.6764	0.4316	0.4464	0.2994
N-C-O	0.4713	0.2673	0.6054	0.5879	0.3926	0.4346	0.5923	0.4089	0.4987	0.3029
N-C=N	0.4598	0.3670	0.3450	0.3986	0.2175	0.3558	0.5498	0.2654	0.3531	0.2593
N-C=O	0.5275	0.3900	0.4285	0.2347	0.2664	0.3690	0.5719	0.3636	0.3695	0.1197
N-N-O	0.8326	0.6048	0.7791	0.7639	0.5862	0.5912	0.7447	0.7117	0.6875	0.4831
N=C-N	0.4598	0.3670	0.3450	0.3986	0.2175	0.3558	0.5498	0.2654	0.3531	0.2593
O=C-N	0.5275	0.3900	0.4285	0.2347	0.2664	0.3690	0.5719	0.3636	0.3695	0.1197

C.2 Lead Optimization

We here give the details of interaction analysis. Since these tasks have provided a partial of the molecules as the context, it is hard to tell the superiority of generated substructures or geometries. Table. 17 and 18 gives details. it shows that

Table 17: Frequency of interaction type on lead optimization tasks.

	Method	hydrophobic	hydrogen	water bridge	π -stacks	π -cation	halogen	metal
	REF.	3.0000	3.0000	0.0000	0.0000	0.0000	0.0000	0.0000
Linker	GRAPHBP	5.5795	2.9812	0.0000	0.5362	0.3537	0.0000	0.0000
	POCKET2MOL	5.1879	3.2759	0.0000	0.1708	0.1082	0.0326	0.0000
	TARGETDIFF	5.3811	3.7133	0.0000	0.1675	0.0827	0.0404	0.0000
	DIFFSBDD	5.4132	3.1350	0.0000	0.1153	0.0132	0.0308	0.0000
	DIFFBP	7.0697	2.6017	0.0000	0.1226	0.0678	0.0204	0.0000
Fragment	GRAPHBP	3.0084	3.2071	0.0000	0.0947	0.0499	0.0196	0.0000
	POCKET2MOL	4.4064	4.0854	0.0000	0.1238	0.0956	0.0131	0.0000
	TARGETDIFF	4.3187	3.6436	0.0000	0.1040	0.0648	0.0405	0.0000
	DIFFSBDD	4.3086	3.6720	0.0000	0.1087	0.0089	0.0468	0.0000
	DIFFBP	5.6128	2.7838	0.0000	0.0552	0.0339	0.0175	0.0000
Side Chain	GRAPHBP	3.0173	1.2207	0.0000	0.2029	0.0321	0.0001	0.0000
	POCKET2MOL	3.0643	3.8911	0.0000	0.0872	0.0708	0.0194	0.0000
	TARGETDIFF	3.3468	3.6206	0.0000	0.0975	0.0527	0.0851	0.0000
	DIFFSBDD	3.6822	3.3479	0.0000	0.0271	0.0242	0.0098	0.0000
	DIFFBP	4.5444	2.5941	0.0000	0.0696	0.0349	0.0141	0.0000
Scaffold	GRAPHBP	0.9560	2.3953	0.0000	0.0000	0.0007	0.0007	0.0000
	POCKET2MOL	3.2220	3.4761	0.0000	0.0282	0.0295	0.0246	0.0000
	TARGETDIFF	3.5427	4.1047	0.0000	0.0612	0.0383	0.0303	0.0000
	DIFFSBDD	4.6225	3.2649	0.0000	0.0021	0.0138	0.1786	0.0000
	DIFFBP	5.0840	2.4424	0.0000	0.0061	0.0055	0.0110	0.0000

Table 18: Distribution of interaction type on lead optimization tasks.

	Method	hydrophobic	hydrogen	water bridge	π -stacks	π -cation	halogen	metal
	REF.	0.5000	0.5000	0.0000	0.0000	0.0000	0.0000	0.0000
Linker	GRAPHBP	0.5904	0.3154	0.0000	0.0567	0.0374	0.0000	0.0000
	POCKET2MOL	0.5912	0.3733	0.0000	0.0195	0.0123	0.0037	0.0000
	TARGETDIFF	0.5734	0.3957	0.0000	0.0178	0.0088	0.0043	0.0000
	DIFFSBDD	0.6216	0.3600	0.0000	0.0132	0.0015	0.0035	0.0000
	DIFFBP	4.1027	1.4830	0.0000	0.0213	0.0039	0.0021	0.0000
Fragment	GRAPHBP	0.4716	0.5027	0.0000	0.0148	0.0078	0.0031	0.0000
	POCKET2MOL	0.5051	0.4683	0.0000	0.0142	0.0110	0.0015	0.0000
	TARGETDIFF	0.5285	0.4459	0.0000	0.0127	0.0079	0.0050	0.0000
	DIFFSBDD	0.5289	0.4508	0.0000	0.0133	0.0011	0.0057	0.0000
	DIFFBP	0.6601	0.3274	0.0000	0.0065	0.0040	0.0021	0.0000
Side Chain	GRAPHBP	0.6746	0.2729	0.0000	0.0454	0.0072	0.0000	0.0000
	POCKET2MOL	0.4296	0.5455	0.0000	0.0122	0.0099	0.0027	0.0000
	TARGETDIFF	0.4647	0.5027	0.0000	0.0135	0.0073	0.0118	0.0000
	DIFFSBDD	0.5192	0.4721	0.0000	0.0038	0.0034	0.0013	0.0000
	DIFFBP	0.6262	0.3575	0.0000	0.0096	0.0048	0.0019	0.0000
Scaffold	GRAPHBP	0.2851	0.7144	0.0000	0.0000	0.0002	0.0002	0.0000
	POCKET2MOL	0.4752	0.5127	0.0000	0.0042	0.0043	0.0036	0.0000
	TARGETDIFF	0.4555	0.5278	0.0000	0.0079	0.0049	0.0039	0.0000
	DIFFSBDD	0.5719	0.4039	0.0000	0.0003	0.0017	0.0221	0.0000
	DIFFBP	0.6735	0.3235	0.0000	0.0008	0.0007	0.0015	0.0000

- The optimization on the side chains has the least effect on the interaction pattern in an overall result and has the greatest influence on the linker.
- GRAPHBP’s failure in scaffold hopping also can be reflected by the fact that the interaction pattern cannot be produced with the molecules.

C.2.1 Case Study

DRD3. For DRD3, we give the distribution of different models’ generated molecules in chemical space in Figure. 7. Different methods capture different clustering centers of the actives, while their distributions show a great gap from the GEOM-DRUG’s randomly sampled molecules.

C.3 Validity

Validity is an important metric to evaluate whether the molecules generated by the models are valid. There are two methods to reconstruct the 3D positions of the atoms into a molecule with bonds, one is used in TARGETDIFF, POCKET2MOL and 3DSBDD, which we name as `Refine`; The second is to use `Openbabel` [61] the software, used in `DiffSBDD`. However, using these methods to reconstruct molecules always carries the risk of broken bonds, which makes the strategy of selecting connected atoms to form fragments and ultimately the final molecule crucial. Here, we define a chemically

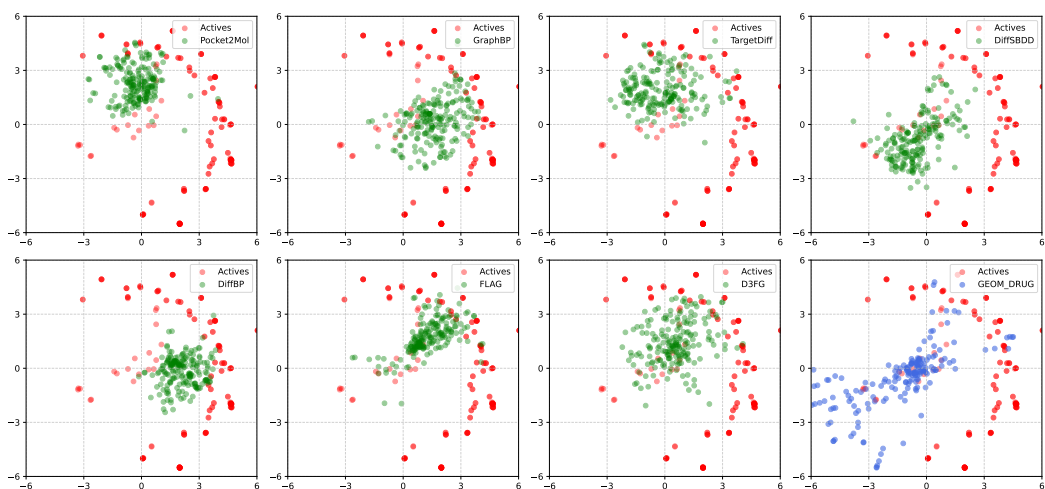


Figure 7: T-SNE visualization of chemical distributions of generated and active molecules on t-SNE.

Table 19: Denovo Validity and Rank

Method	Validity	Rank
LiGAN	0.42	10
3DSBDD	0.54	9
GraphBP	0.66	8
Pocket2Mol	0.75	5
TargetDiff	0.96	1
DiffSBDD	0.71	6
DiffBP	0.78	3
FLAG	0.68	7
D3FG	0.77	4
DecompDiff	0.89	2

valid molecule as one where the number of atoms in the largest fragment is greater than 85% of the total number of atoms, and we use this as the criterion for the reconstruction. Additionally, we employed a ‘Refine + Openbabel’ strategy, where if refinement is unsuccessful, Openbabel is added as a reconstruction method. Under this definition, the validity of various methods in the *de novo task* is shown in Table. 19. DecompDiff and TargetDiff have the highest validity.